Nanoindentation Analysis of Mechanical Property Statistics of Canine Bone Tissue

Eugene S. Statnik, Alexei I. Salimon, Yuliya V. Kan, Julijana Cvjetinovic and Alexander M. Korsunsky, *Member, IAENG*

***Abstract*— This paper presents the analysis of data obtained using nanoindentation mapping of a canine bone section using a Berkovich tip. The experiments were carried out to investigate the mechanical properties of bone as an example of a natural inhomogeneous composite material. In order to obtain insight into the mechanical contributions of collagen and hydroxyapatite (HAp), the principal natural constituents of the bone tissue, specimens of natural and deimmunized bones were studied. The analysis of the indentation data returns estimates of Young's modulus and hardness at different locations within the bone structure. The observed variation of mechanical properties is discussed.**

***Index Terms*— Canine bone, collagen, hardness, hydroxyapatite, modulus of elasticity, nanoindentation**

I. Introduction

BONE is a diverse tissue having a complex, highly porous and multiscale structure which mechanical properties depend on the architecture and intrinsic material properties [1, 2]. Besides, it is responsible for the wide set of functions from mobility to vital organ protection. A large number of studies in the literature report the investigation of the dependence of bone macro-scale mechanical properties on tissue architecture [3]. However, even when finer scale properties are considered within a selected part of the bone, the mechanical properties vary continuously as a reflection of hierarchical structuring down to the nanoscale due to the permanent processes of bone remodeling and adaptation to an external load. Hence, the microscale irregularities of structure make an impact on the characteristics of composite [4]. Accordingly, the knowledge of the mechanical properties of bone plays an essential role in understanding such complex phenomena as the implant-bone interaction, bone diseases, and fractures [5].

Manuscript received April 08, 2019; revised April 19, 2019.

E.S. Statnik is with AMT, Skoltech Advanced Manufacturing Technologies, Skolkovo Institute of Science and Technology, Nobel St., 3, Moscow, Russia 121205, e-mail: eugene.statnik@skoltech.ru

A.I. Salimon is with CEE, Skoltech Center for Electrochemical Energy Storage, Skolkovo Institute of Science and Technology, Nobel St., 3, Moscow, Russia 121205, e-mail: a.salimon@skoltech.ru

Yu.V. Kan is with CEE, Skoltech Center for Electrochemical Energy Storage, Skolkovo Institute of Science and Technology, Nobel St., 3, Moscow, Russia 121205, e-mail: yuliya.kan@skoltech.ru

J. Cvjetinovic is with NUST "MISiS", 119049, Russia, Moscow, Leninsky Prospekt, 4, e-mail: julijana.cvjetinovic@gmail.com

A.M. Korsunsky is Head of MBLEM, the University of Oxford, Department of Engineering Science, Oxford OX1 3PJ; e-mail: alexander.korsunsky@eng.ox.ac.uk; and with Skolkovo Institute of Science and Technology, Nobel St., 3, Moscow, Russia 121205

The mechanical properties of bone tissue are correlated with its structure and orientation with respect to the direction of load application. Due to the density difference between the cortical bone and cancellous bone, the former exhibits higher modulus (12-20 GPa vs 0.2-0.8 GPa) and strength (100-230 MPa vs 2-12 MPa) [6]. The specific organization of tissue microstructure results in strong anisotropy of mechanical properties. For instance, the cortical bone elastic modulus is ~18 GPa under axial force application, and 12 GPa under transverse loading, respectively [7].

The measurements of Young's modulus and hardness of highly heterogeneous materials by a statistical analysis of instrumented indentation techniques have widely been adopted and used for the characterization of nanomechanical behavior of mineralized tissues [9-11]. Advantages arise from precise geometric positioning of the indenter tip on the sample, allowing correlation between mechanical response and local microstructure. The interpretation of the load-displacement record provides precise values of elastic modulus and hardness. The range of properties corresponding to specific phases can be identified by performing large arrays of indentations in highly heterogeneous samples, with a proper choice of the indentation conditions in terms of load and depth [12].

The main goal of this investigation is to verify the conceptual model of bone tissue as a composite material that consists of collagen and hydroxyapatite (HAp) as the principal phases. Thorough statistical analysis of large experimental nanoindentation datasets reveals the nature of bone property inhomogeneity.

II. Materials and Methods

A. Bone Preparation

In this study shinbone tissue specimens were used that were taken from an ethically mortified dog (presented by NMRCO named N.N. Blokhin, Moscow, Russia). The dog had undergone a bone surgery, namely, the resection of a sarcoma-affected segment, and further bone reconstruction with a titanium-polymer hybrid implant. The implant was externally supported by titanium plates fixed with titanium screws. Consequently, the specimen contained drilled holes which corresponded to the location of screws fixed into the bone tissue (Fig. 1). In addition, a sample was prepared from another shinbone by etching deimmunized in a water-based solution (5-10 wt.%) prepared from a dry mixture of sodium chlorite, sodium perchlorate, and sodium chloride in the ratio of 7:2:1, and distilled water [14].

ISBN: 978-988-14048-6-2
ISSN: 2078-0958 (Print); ISSN: 2078-0966 (Online)

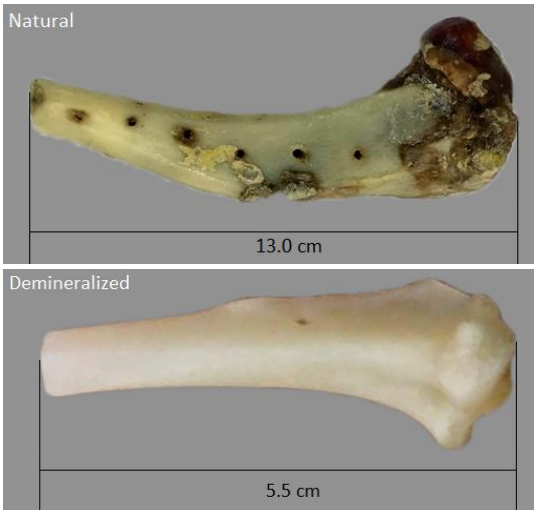

Fig. 1. The specimens of canine bone.

Sample preparation procedure and testing conditions may significantly affect the results of the nanoindentation. This is particularly relevant for biological tissues due to the irregular shape and fixation of specimens. The mechanical characteristics also depend on the water content, resulting in up to 40% difference in measured indentation modulus for compact and trabecular bone [13]. At the preliminary step, bones were cut in the vicinity of the drilled holes used for titanium plate fixation in the bone surgery operation. Accutom-100 (Struers Ltd, UK) with a diamond cutting disk was used for sectioning, with the rotation speed of 1 mm/min with a continuous supply of coolant fluid. After cutting (Fig. 2), the specimens were dried in Binder FD115 (Thomas Scientific, US) during 12 hours at 40 °C in order to avoid the enzymatic degradation of bone collagen matrix due to water.

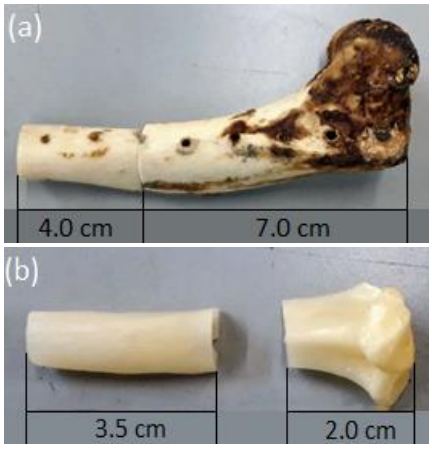

Fig. 2. Natural (a) and deimmunized (b) samples after sectioning.

The samples were then encapsulated in black phenolic resin mounting using hydraulic-pneumatic automatic mounting press TechPress 2™ (Allied Company, USA). Samples were shaped into cylinders of 20 mm height and 30 mm diameter, respectively (Fig. 3). Surface preparation was carried out by MetPrep 3™ (Allied Company, USA) by grinding and polishing with a set of abrasives under constant water flow. The surface was finished with colloidal silica suspension OP-S Nondry (Struers Ltd, UK) of nominal spherical particle size 40 nm. The quality of surface finishing was monitored by means of confocal laser profilometer NanoScan-4D Company (TISNCM, Troitsk, Russia). Grinding resulted in the roughness R_z of 3.925 μm.

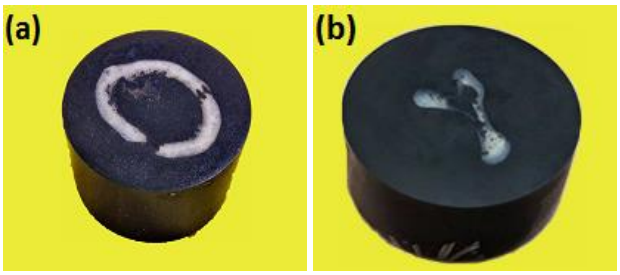

Fig. 3. The natural (a) and HAp free (b) canine bone tissue mounted in epoxy resin.

B. Nanoindentation Testing

Nanoindentation tests were performed at room temperature using a NanoScan-4D scanning nanohardness tester (TISNCM, Troitsk, Russia) using Berkovich tip in the load-controlled mode. Three areas of cortical bone were investigated: A - zone close to drilled hole; B - outer region, and C - inner zone, respectively (Fig. 4).

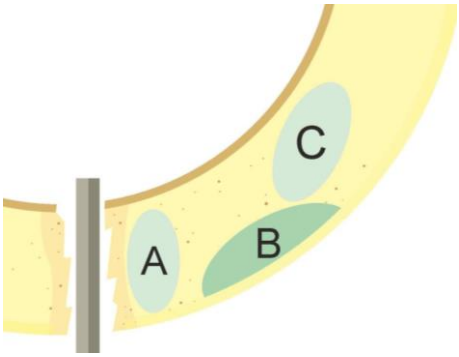

Fig. 4. The three test locations: A – zone close to drilled hole, B – outer side of bone and C – inner zone of bone.

Maximum indentation load of 50 mN was applied. The loading and holding durations were set as 10 and 0.5 s, respectively, with unloading carried out at the same force ramp rate as the loading. The total of 1000 measurements were made in the A, B and C zones (Fig. 5), and about 250 were performed on the demineralized sample (zone D). The tests were interpreted according to the method of Oliver and Pharr [15]. According to this approach, the elastic unloading stiffness S is defined as the slope of the unloading curve during the initial stages of unloading. A typical nanoindentation load-depth curve is illustrated in Fig.6.

ISBN: 978-988-14048-6-2
ISSN: 2078-0958 (Print); ISSN: 2078-0966 (Online)

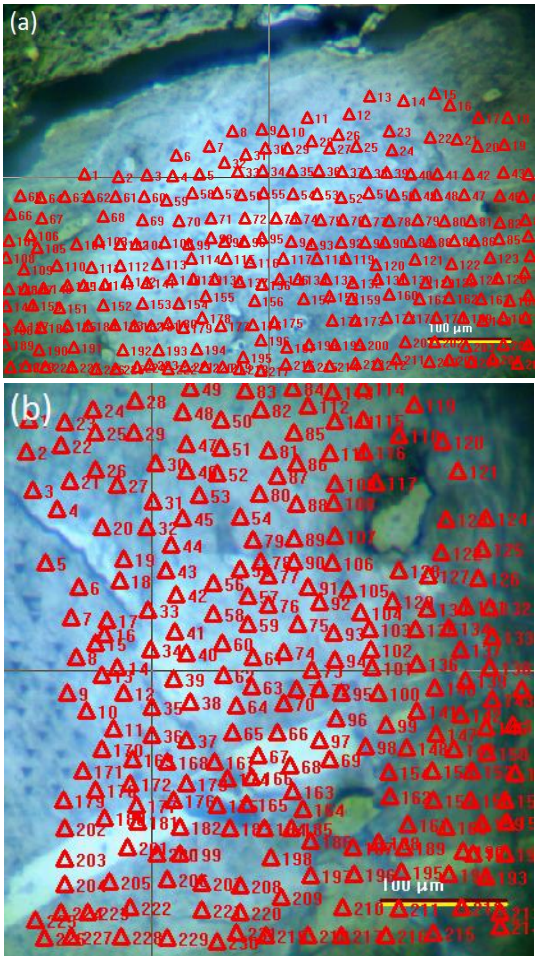

Fig. 5. The indent grids in zones C (a) and B (b).

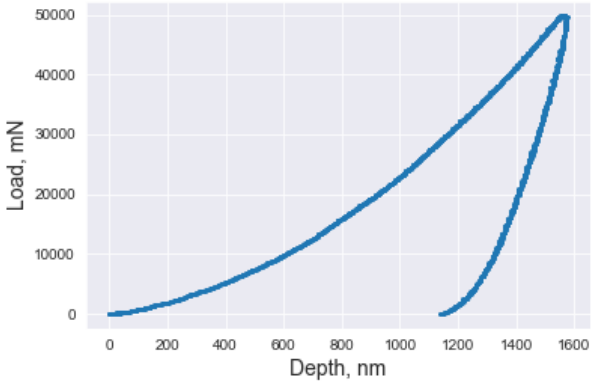

Fig. 6. Typical indentation load-displacement curve.

The relationship between the stiffness S, the contact area A, and the reduced elastic modulus E_r is given by

$$S = \frac{2}{\sqrt{\pi}} E_r \sqrt{A}, \tag{1}$$

and relationship between Young's modulus and Poisson's ratio of the diamond tip E_i, ν_i with Young's modulus and Poisson's ratio of the tested material E_s, ν_s is

$$\frac{1}{E_r} = \frac{1-\nu_i^2}{E_i} + \frac{1-\nu_s^2}{E_s}. \tag{2}$$

C. Statistical Analysis Technique

For the interpretation of nanoindentation results, statistical analysis was applied to generate the Probability Density Function (PDF). For the purposes of recognizing specific phase contributions, a fit to the PDF was sought in the form of a sum of Gaussian functions for [16]:

$$P(X) = \eta \sum_{i=1}^{n} f_{ji} \frac{1}{\sigma_i \sqrt{2\pi}} \exp\left(-\frac{(X-\mu_i)^2}{2\sigma_i^2} \right) \tag{3}$$

where η is scale factor (e.g. a number of nanoindentation tests), n is the number of different phases, f_{ji}, σ_i and μ_i represent the volume/surface fraction occupied by the i-th phase, and the standard deviation and the mean values of the i-th phase, respectively.

The best fit was found by minimizing the standard error

$$\sum_{i=1}^{m} \frac{\left[Y(X_j) - P(X_j) \right]^2}{m}, \text{ where } \sum_{j=1}^{n} f_j = 1, \tag{4}$$

and X_j, $Y(X_j)$ are the j-th abscissa and ordinate values of the experimental results, respectively.

III. Results and Discussion

A typical appearance of the cortical bone tissue cross-section under optical microscope is shown in Fig. 7. A number of structure elements can be noted: lacunae (zones surrounding blood vessel channels) with an approximate size of about 150-200 µm, a system of cracks of ~1-10µm width, and canaliculi, visible as black spots of diameters 5-10 µm. The previously reported approach to the statistical analysis of large nanoindentation datasets [17] allows identifying a number of mechanical phases, and establishing correspondence with these or other, possibly optically unresolvable structural elements.

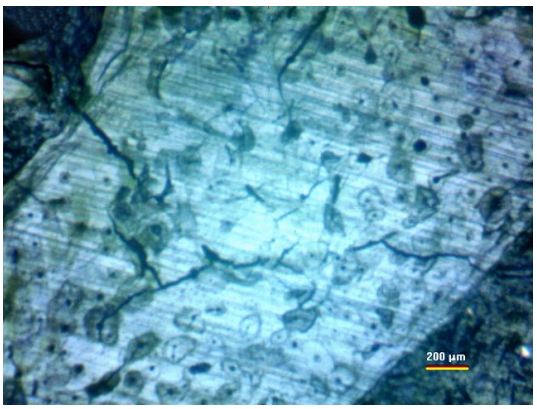

Fig. 7. A typical appearance of cortical bone tissue.

ISBN: 978-988-14048-6-2
ISSN: 2078-0958 (Print); ISSN: 2078-0966 (Online)

Images of indent grids covering 300x300 μm areas, as well as hardness and elastic modulus maps in B and C zones are illustrated in Fig. 8. They include several decades of structural elements and so it is believed that datasets should be sufficiently representative to resolve different mechanical phases in a statistically reliable manner.

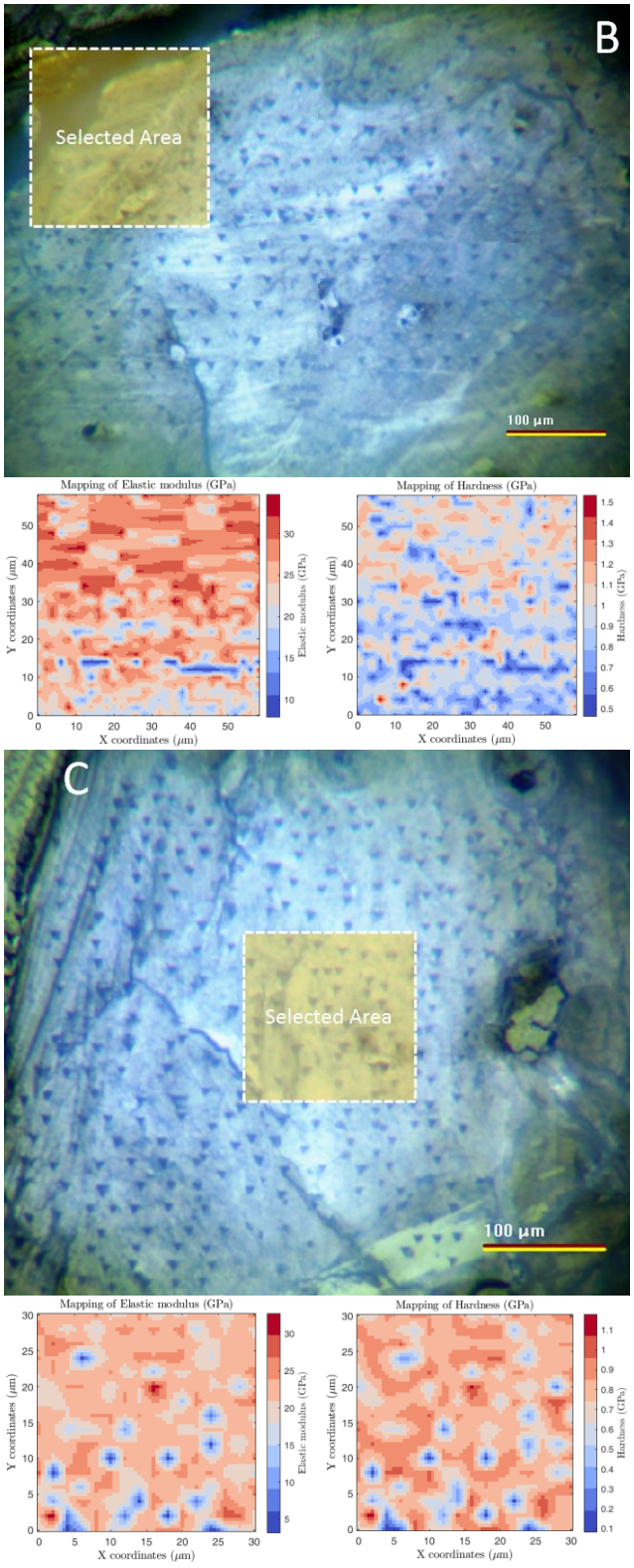

Fig. 8. The hardness and Young's modulus maps in zones B and C of natural (deimmunized).

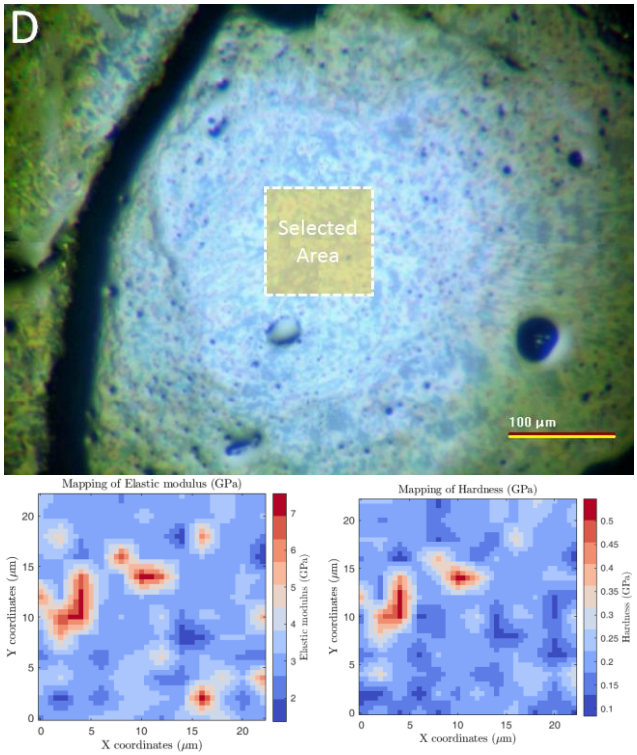

Fig. 9. The hardness and Young's modulus maps in zones B and C of demineralized bone.

The histograms of the hardness and Young's modulus values show evidence of the presence of mechanical phases with distinct properties (Fig. 10). It appears possible to resolve the statistic of mechanical response into a convolution of Gaussian histograms from at least three mechanical phases. The estimates of their mechanical properties are given in the Table 1, where the putative phases are denoted Phase 1, 2 and 3, respectively.

Table 1. The mechanical characteristics of suggested mechanical components.

Property	Phase 1	Phase 2	Phase 3
E, GPa	13±2	22±2	27±3
H, GPa	0.5±0.05	0.7±0.04	0.9±0.05

The convolution of histograms, however, cannot be directly interpreted as an additive summation of mechanical properties of mechanical phases with some weights reflecting the contribution of mechanical phases to the mechanical properties of the composite material in accordance with a rule of mixtures. The anisotropy of bone mechanical properties arises due to a variety of mechanisms, e.g. texture (preferred orientation) of HAp grains, uneven mineralization along different directions, uneven porosity, etc. Sophisticated numerical modelling (homogenization) is required in order to describe the mechanical properties even at micrometer dimensional level.

ISBN: 978-988-14048-6-2
ISSN: 2078-0958 (Print); ISSN: 2078-0966 (Online)

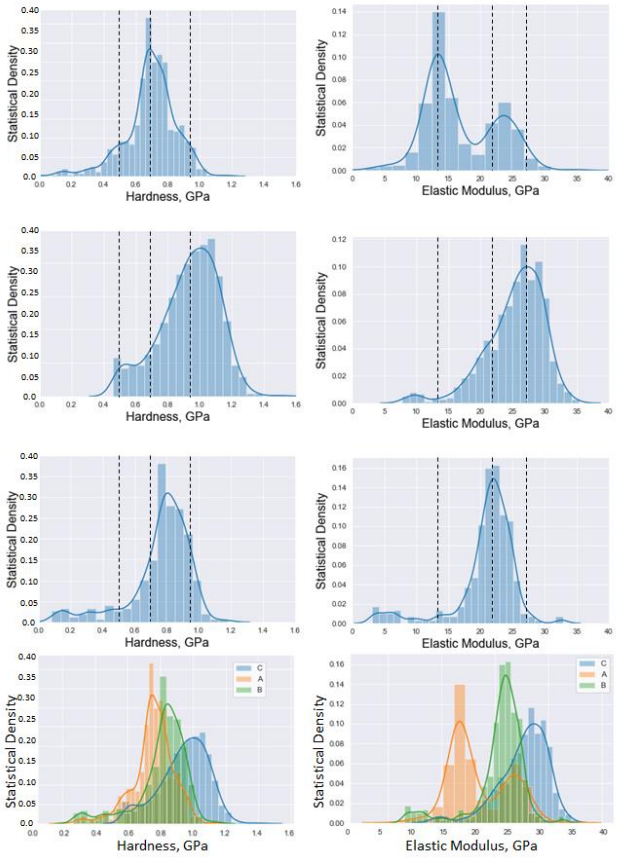

Fig. 10. Histograms of mechanical properties of natural (deimmunized) canine bone: a) zone A, b) zone B, c) zone C.

Some speculations, nevertheless, can be made when structure elements of bone tissue are considered. We believe that the least rigid and hard Phase 1, which mostly present in zone A, is also the least mineralized and contains many defects – pores, cracks etc. as result of trauma due to the interaction with titanium screws and other fixing elements. We relate the highest mechanical performance in zone B with the highest content of Phase 3, that is thought of as an almost defect-free structure with average to higher mineralization. In fact, lacunae and canaliculi are much less frequently found in the outer bone zone, making it harder and more rigid. Area C corresponds to Phase 2 that shows intermediate mechanical properties, likely due to somewhat lower mineralization and high content of lacunae and canaliculi (Fig. 8 shows a softer fragment related to canaliculi in zone C). Improved statistics of at least 5000 indents per dataset for each area can be expected to allow making more reliable conclusions for numerical homogenization.

Demineralized bone tissue appears to have two mechanical phases with strong domination of a stiffer phase with Young's modulus of 3±0.5 GPa and hardness 0.2±0.05 GPa, as shown in Fig. 11.

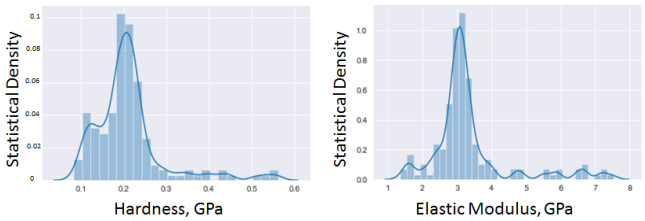

Fig. 11. Demineralized bone mechanical properties histogram.

Modelling of the mechanics of cortical bone tissue as a composite material consisting of two main components – collagen and HAp - is a challenging task even for almost pure HAp objects, such as tooth enamel, since it requires a hierarchical approach that takes into account complex multi-scale structural features and texture of HAp nanometer size grains [18]. Addressing this challenge for bone tissue demands rigorous and systematic multi-scale structural characterization and more representative statistics to evaluate the mechanical properties of differently mineralized structural elements, such as the regions surrounding lacunae and canaliculi. In Fig. 12 we demonstrate that the simple rule of mixture is not directly applicable for collagen/HAp composite objects – the mechanical properties in the array of pure collagen, bones (40-60 % of HAp) and tooth enamel (almost pure HAp) are almost linearly dependent on HAp content on a logarithmic scale, rather than linear scale.

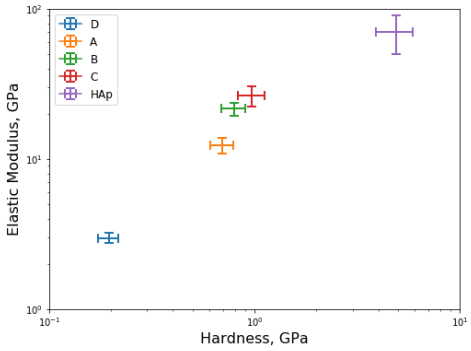

Fig. 12. Ashby chart for mechanical performance of natural collagen/HAp composite objects – bones and HAp [19].

IV. Conclusion

The application of statistically representative nanoindentation measurements (many thousands) facilitated by modern automated experimental instruments returns large datasets for sophisticated analysis of structure-properties relations. For cortical bone tissue, mechanically distinct phases can be identified and ascribed to structural elements – A) demineralized areas enriched with defects in the vicinity of macroscopic damage, C) composite areas with lacunae and canaliculi, and B) relatively defect-free outer areas of bone. Large datasets also provide relevant information for numerical homogenization as part of detailed computer simulation of bone mechanical behavior.

ISBN: 978-988-14048-6-2
ISSN: 2078-0958 (Print); ISSN: 2078-0966 (Online)

ACKNOWLEDGMENT

Authors are grateful to Royal Society (Grant IEC/R2/170223) for financial support.

REFERENCES

[1] A. R. Amini, C. T. Laurencin, and S. P. Nukavarapu, "Bone tissue engineering: recent advances and challenges," *Crit. Rev. Biomed. Eng.*, vol. 40, 2012, pp. 363–408.
[2] D. Wu, P. Isaksson, S. J. Ferguson, and C. Persson, "Young's modulus of trabecular bone at the tissue level," *Acta Biomaterialia*, vol. 78, 2018, pp. 1–12.
[3] J. Y. Rho, L. Kuhn-Spearing, and P. Zioupos, "Mechanical properties and the hierarchical structure of bone," *Med. Eng. Phys.*, vol. 20, 1998, pp. 92–102.
[4] D. Bajaj, J. R. Geissler, M. R. Allen, D. B. Burr, and J. C. Fritton, "The resistance of cortical bone tissue to failure under cyclic loading is reduced with alendronate," *Bone*, vol. 64, 2014, pp. 57–64.
[5] B. P. Hung, D. L. Hutton, and W. L. Grayson, "Mechanical control of tissue-engineered bone," *Stem Cell Reserch & Therapy*, vol. 4, 2013, pp. 1–10.
[6] M. Fröhlich, W. L. Grayson, L. Q. Wan, D. Marolt, M. Drobnic, and G. Vunjak-Novakovic, "Tissue engineered bone grafts: biological requirements, tissue culture and clinical relevance," *Stem Cell Research & Therapy*,, vol. 3, 2008, pp. 254–264.
[7] R. Karpiński, Ł. Jaworski, and P. Czubacka, "The structural and mechanical properties of the bone," *Journal of Technology and Exploitation in Mechanical Engineering*, vol. 3, 2017, pp. 43–50.
[8] E. Mittra, S. Akella, and Y. X. Qin, "The effects of embedding material, loading rate and magnitude, and penetration depth in nanoindentation of trabecular bone," *Journal of Biomedical Materials Research*, vol. 79A, 2006, pp. 86–93.
[9] J. A. Ortega, F. J. Ulm, and Y. Abousleiman, "The effect of the nanogranular nature of shale on their poroelastic behavior," *Acta Geotechnica*, vol. 2, 2007, pp. 155–182.
[10] C. Bobko and F. J. Ulm, "The nano-mechanical morphology of shale," *Mechanics of Materials*, vol. 40, 2008, pp. 318–337.
[11] K. Tai, F. J. Ulm, and C. Ortiz, "Nanogranular Origins of the Strength of Bone," *Nano Letters*, vol. 6, 2006, pp. 2520–2525.
[12] F. J. Ulm, M. Vandamme, C. Bobko, J. Alberto Ortega, K. Tai, and C. Ortiz, "Statistical Indentation Techniques for Hydrated Nanocomposites: Concrete, Bone, and Shale," *Journal of the American Ceramic Society*, vol. 90, 2007, pp. 2677–2692.
[13] A. K. Bembey, M. L. Oyen, A. J. Bushby, and A. Boyde, "Viscoelastic properties of bone as a function of hydration state determined by nanoindentation," *Philosophical Magazine*, vol. 86, 2006, pp. 5691–5703.
[14] N. Yu. Anisimova, F. V. Donenko, and M. V. Kiselevskiy, "Method for producing bioengineered construct for bone defect replacement," Russian Federation Patent RU2644828C1, May 27, 2013.
[15] W. C. Oliver and G. M. Pharr, "An improved technique for determining hardness and elastic modulus using load and displacement sensing indentation experiments," *Journal of Materials Research*, vol. 7, 1992, pp. 1564–1583.
[16] T. H. Pham and S. E. Kim, "Nanoindentation for investigation of microstructural compositions in SM490 steel weld zone," *Journal of Constructional Steel Research*, vol. 110, 2015, pp. 40–47.
[17] M. Sebastiani, K. E. Johanns, E. G. Herbert, and G. M. Pharr, "Measurement of fracture toughness by nanoindentation methods: Recent advances and future challenges," *Curr. Opin. Sol. State Mater. Sci*., vol. 19, 2015, 324-333.
[18] T. Sui and A. M. Korsunsky, "Hierarchical Modeling of Elastic Behavior of Human Dental Tissue Based on Synchrotron Diffraction Characterization," *Advanced Healthcare Materials*, 2014, pp. 237-268.
[19] V. V. Silva, F. S. Lameiras, and R. Z. Domingues, "Microstructural and mechanical study of zirconia-hydroxyapatite (ZH) composite ceramics for biomedical applications," *Composites Science and Technology*, vol. 61, 2001, pp.301–310.

ISBN: 978-988-14048-6-2
ISSN: 2078-0958 (Print); ISSN: 2078-0966 (Online)